CHEMICAL ENGINEERING TRANSACTIONS
VOL. 105, 2023
A publication of AIDIC
The Italian Association of Chemical Engineering
Online at www.cetjournal.it
Guest Editors: David Bogle, Flavio Manenti, Piero Salatino

ISBN 979-12-81206-04-5; **ISSN** 2283-9216
DOI: 10.3303/CET23105049

Hydrodynamics and Scale-up of Anaerobic Stirred Digesters

Francesco Maluta, Federico Alberini, Alessandro Paglianti, Giuseppina Montante*

Dipartimento di Chimica Industriale "Toso Montanari", Alma Mater Studiorum Università di Bologna, viale Risorgimento 4, 40136 Bologna, Italy
giuseppina.montante@unibo.it

The investigation presented in this work is aimed at providing a detailed characterization of the hydrodynamics in a digester of typical design, considering different scale-down criteria for the selection of the agitation conditions, with the final purpose of suggesting a methodology for aiding in reducing the energy demand of the digesters while optimizing the biogas production rates. A stirred tank of 40 litres having the same geometry of an industrial digester of 1500 m^3 is investigated by means of experiments and simulations. A model fluid mimicking the rheological behaviour of the digester content stirred in a biogas production plant, which exhibits a pseudo-plastic behaviour, is adopted. The velocity field obtained from Particle Image Velocimetry and the results of Computational Fluid Dynamics simulations are discussed, focusing on well-known critical hydrodynamic features for the biogas production, namely low-velocity zones, velocity gradients and shear stresses. The detailed fluid dynamics analysis can contribute to improve the equipment design, to optimize the energy requirement and to avoid failure of the biogas production due to poor or improper mixing of the feedstock.

1. Introduction

Anaerobic digestion is increasingly adopted for the production of biogas from agricultural scraps and waste materials in several countries. Some of the advantages of the biogas production processes are related to the flexibility in converting very diverse carbon sources, leading to a straightforward integration with different food and agricultural productions (Theuerl et al., 2019). Improvements of biogas plant performances can be expected from deeper knowledge and innovations on many aspects, such as the combination of different feedstocks (Moretta et al., 2022), the pre-treatment operations (Battista et al., 2014) and the biogas upgrading (Scamardella et al., 2019) to name a few. Improvements can be also expected from robust methodologies for extending the lab-scale results to the production scale, taking into account the fluid dynamics in the digesters and its coupling with the rheology of the digestate and the biogas production. As pointed out in many recent investigations, biogas production in wet digesters can be significantly affected by the agitation mode (Singh et al., 2019), which in turn depends on the interplay of geometrical, physical and operating variables. In this work, state-of-art experimental and computational methods are adopted to analyse typical features of anaerobic digester hydrodynamics, such as low-velocity zones (Leite et al., 2023), shear stresses (Lebranchu et al., 2017) and velocity gradients (Dabiri et al., 2021). As a difference with previous experimental works (Alberini et al., 2023), a preliminary rheological characterization of a sample of the anaerobic slurry taken from a production digester of design identical to that of the investigated stirred tank is performed, for guiding towards a close representation of the production operating conditions.

2. Material and Methods

The investigated stirred tank is obtained from the geometrical scale-down of a digester for the production of biogas from agricultural scraps installed in Emilia Romagna and it can be considered as representative of a typical geometrical configuration adopted in biogas production plants. It consists of a cylindrical tank stirred with three top-entering shafts set symmetrically with respect to the vessel axis, each provided with six inclined blades. For the Computational Fluid Dynamics (CFD) simulations, the domain depicted in Figure 1(a) is adopted, which closely matches the laboratory geometry, apart from a simplification on the shape of the

Paper Received: 31 January 2023; Revised: 22 May 2023; Accepted: 18 July 2023
Please cite this article as: Maluta F., Alberini F., Paglianti A., Montante G., 2023, Hydrodynamics and Scale-up of Anaerobic Stirred Digesters, Chemical Engineering Transactions, 105, 289-294 DOI:10.3303/CET23105049

blades, which are flat in the simulations. The blade shape in the production and in the scale-down vessels is slightly curved, as shown in Figure 1(b). In both the experiments and the simulations, the blade tip is inclined of 45° with respect to the horizontal. The three lower blades are mounted with opposite inclination with respect to the upper, as in the production fermenter. As a result, up-pumping agitation is provided with the three lowest blades and down-pumping agitation with the three highest blades. The diameter swept by each blade, D, is equal to 84mm.

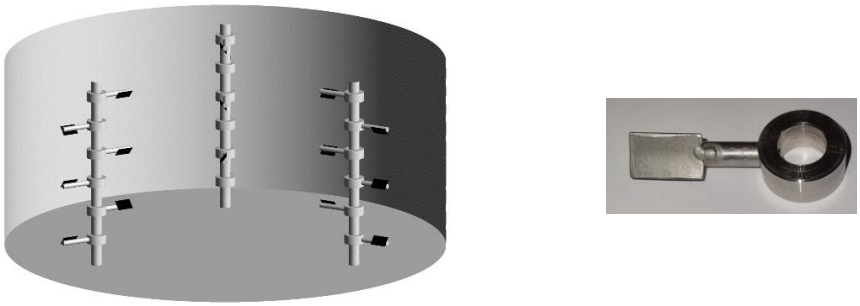

(a) (b)

Figure 1: Sketch of the stirred vessel geometry adopted for the CFD simulations (a) and picture of one of the blades adopted in the experiments (b).

Two fluids are considered for the simulations, a sample taken from the production digester, which will be referred to as digestate in the following, and an aqueous solution of 8 g/L of Carboxy-methylcellulose (CMC). The latter fluid is also adopted in the experiments. Both the fluid's rheology follows the Ostwald-de-Waele constitutive equation:

$$\tau = k_s \dot{\gamma}^n \quad (1)$$

With τ being the shear stress, $\dot{\gamma}$ the strain rate, k_s the consistency index and n the flow behavior index. The density, ρ, and the rheological constants are listed in Table 1. They were measured at 20°C temperature for the model fluid, that is the temperature adopted in the experiments, and at 40°C for the digestate sample, that is the digestion temperature.

Table 1: Physical properties of the digestate (T=40°C) and the aqueous CMC solution (T=20°C)

Fluid	ρ [kg/m^3]	k_s [Pa·s^{2-n}]	n [-]
CMC in water	998	4.22	0.44
Digestate	980	63.56	0.28

The constant tip speed and the constant shear rate criteria are used for selecting the impeller speed in the laboratory scale, considering that the biogas production is carried out at the impeller speed, N, of 10.5 rpm. The former corresponds to N=366 rpm (constant ND) and the latter, based on the correlation of Wichterle et al. (1984), is equal to N=122rpm (constant ND$^{2/3}$).

2.1 The measurement system

The instrumentation adopted for the velocity field measurements consisted of a Particle Image Velocimetry (PIV) system, including a Nd:YAG Litron DualPower Laser (light wavelength, λ = 532 nm, 60 mJ/pulse), one Hi Sense MKII camera (1344 × 1024 pixel resolution) and a Dantec Dynamics data acquisition system. The laser light sheet approximately 2 mm thick enters the vessel horizontally through the tank lateral wall at the elevation of the second blades from the vessel bottom (z=63mm). To guarantee a sufficient spatial resolution, the measurement areas is limited to the plane portion close to one blade. The flow was seeded with silver-coated hollow glass particles of mean diameter equal to 10 μm. The vessel is placed within a larger square vessel made of Perspex filled with the working liquid in order to minimize optical distortion of the laser light. The analysis of the instantaneous image pairs is carried out by an adaptive-correlation algorithm, applied on interrogation areas (IA) of initial size 64 x 64 pixel and final size of 16 x 16 pixel, allowing the reconstruction of the flow field with a spatial resolution of 1.4 mm. Two validation thresholds, one based on the evaluation of the peak heights in the correlation plane and the other on the velocity magnitude are adopted. The time interval between two laser pulses is set with the usually adopted criteria for the PIV experimental error minimization. The ensemble averaged velocity field is obtained averaging 1000 image pairs, which ensures statistical convergence of the mean velocities. The ensemble averaged velocity magnitude on the horizontal plane, $|V|$, obtained from the two velocity components parallel to the plane, u and v, is:

$$|V| = \sqrt{u^2 + v^2} \tag{2}$$

2.2 The computational method

The fluid velocity field is predicted by solving the unsteady, incompressible, isothermal Navier-Stokes equations:

$$\nabla \cdot (\rho \boldsymbol{u}) = 0 \tag{3}$$

$$\frac{\partial u}{\partial t} + \nabla \cdot (\rho \boldsymbol{u}\boldsymbol{u}) = \nabla \cdot \sigma - \nabla P \tag{4}$$

Where $\boldsymbol{u}$ is the fluid velocity vector, P is the pressure, and σ is the laminar shear stress, equal to:

$$\sigma = \mu_a \dot{\gamma} \tag{5}$$

$\dot{\gamma}$ is obtained from the velocity gradients as:

$$\dot{\gamma} = (\nabla \boldsymbol{u} + \nabla \boldsymbol{u}^T) \tag{6}$$

and the apparent viscosity μ_a is obtained from Eq. (1), as:

$$\mu_a = k_s \dot{\gamma}^{n-1} \tag{7}$$

The equations are numerically solved in a Cartesian coordinate system running the finite volume CFD code ANSYS FLUENT 2021 R1. The computational grid consists of about 1.6×10^6 cells and it is refined close to the blades. The inner part of the domain extends from the bottom to the top of the vessel and contains the shafts and the blades. It consists of three rotating reference frames, where the shafts are steady, while a steady reference frame is used for the rest of the vessel. For the coupling between the rotating and the steady domain the Sliding Mesh (SM) method is adopted, with 120 time steps per revolution and 30 internal iterations per time step. The simulation of about 12 seconds of real time shaft rotation starting from still fluid ensures the achievement of the pseudo-steady state solution. The solution convergence is carefully checked by monitoring the residuals of all variables, which are dropped to the order of 10^{-4} or less, and the physical values of the velocity close to one of the blades. After obtaining a fully developed flow field, the results are time averaged on the last 120 time steps for performing a consistent comparison with the PIV data. Just for one condition, the simulation with the steady Multiple Reference Frame (MRF) is also carried out, to assess the differences with the SM results. Further details on the numerical solution strategy are omitted for the sake of conciseness.

Results and discussion

The experimental velocity magnitude on the plane section including one of the blades and the vessel wall at the two impeller speeds, each normalized with the maximum velocity value, is depicted in Figure 2. The very strong velocity reduction moving far from the shaft axis is apparent, with different features at the two values of N. In the case of N=366 (Figure 2a), the velocity exhibits a maximum value at a radial coordinate from about 20 mm to 40 mm from the shaft axis, while at N=112rpm (Figure 2b), the fluid has maximum velocity from the shaft axis up to about 35 mm, than it decreases to very low values.

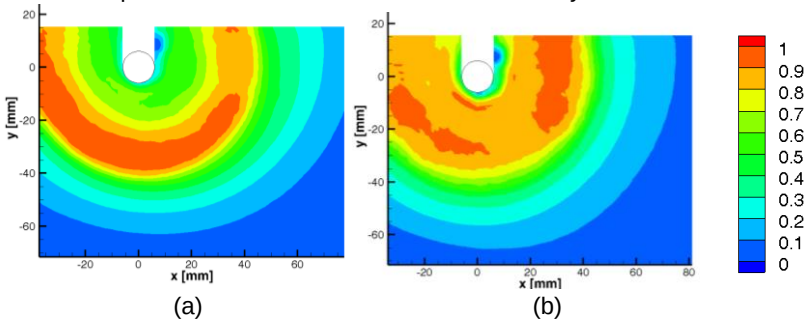

(a) (b)

Figure 2: Map of the normalized magnitude of the CMC solution in plane velocity components measured on the horizontal section close to one shaft located at z=63mm. (a) N=366 rpm (V_{tip}=cost); (b) N=122rpm (maximum shear rate=cost).

The same flow features are observed in the predicted maps depicted in Figure 3 (a) and (b), which are obtained with the time dependent SM method. The agreement between the experimental and computational

results indicates that quite robust guidelines can be obtained from the CFD simulation on the hydrodynamics variables affecting the biogas production, even with relatively small simplification of the real geometry. Instead unphysical results, which depends on the location of the impeller blades, are obtained with a steady approach, as shown in Figure 3(c), where the MRF results are depicted. The results confirm that the significantly different numerical and modelling methodologies are required for unbaffled tanks stirred with eccentric agitators (Montante et al., 2006) and baffled tanks (Maluta et al., 2019).

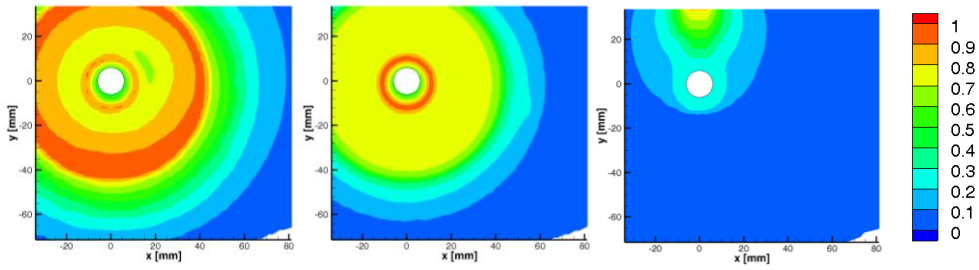

Figure 3: Maps of the normalized magnitude of the CMC solution in plane velocity components as obtained from the simulation in the same section of Figure 2. (a) N=366 rpm (V_{tip}=cost); (b) N=122rpm (maximum shear rate=cost); (c) N=366 rpm (MRF simulation).

The robustness of the computational method is further assessed by the comparison of the dead zones obtained from the experimental and the computed SM results in Figure 4. As can be observed, the percentage value of dead zones, defined following Bridgeman (2012) and considering the maximum velocity equal to the impeller tip speed, v_{tip}, is well predicted in both cases. Of the two criteria, the constant tip speed leads to a better velocity distribution, being about equal to 20% the portion of the observed section with values of velocity lower than the 5% of the maximum velocity, while with at constant shear rate it is about doubled.

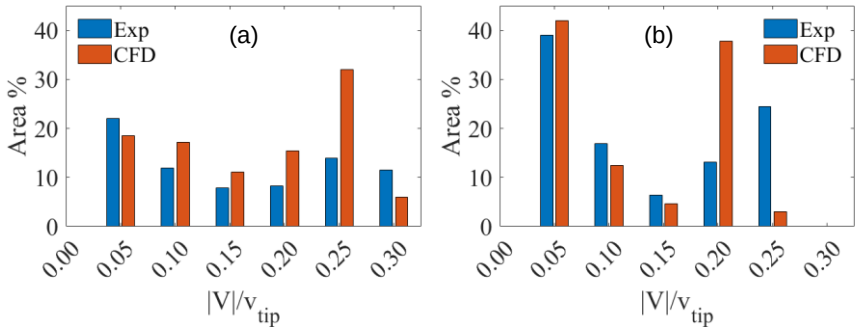

Figure 4: Dead zones distribution on the vessel section of Figure 2. (a) N=366 rpm (V_{tip}=cost); (b) N=122rpm (maximum shear rate=cost).

The velocity magnitude, the apparent viscosity and the shear rate obtained at the two impeller speeds on the entire vessel section located at the elevation of the second blade from the bottom are depicted in Figure 5 and 6, to provide an indication of the significant variation of the hydrodynamics characteristics that can be expected depending on the impeller speed, due to the pseudo-plastic behaviour of the stirred fluid.

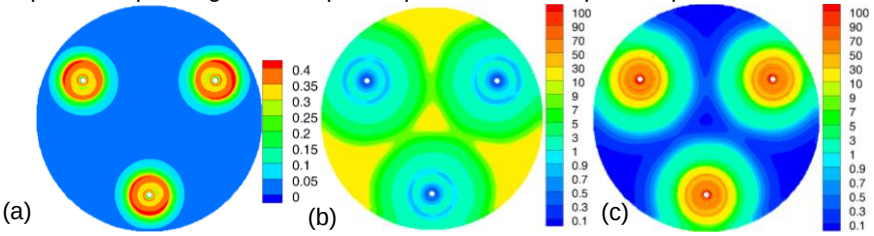

Figure 5: Predicted maps of the CMC solution velocity magnitude [m/s] (a), the viscosity [Pa·s] (b) and the shear rate [s^{-1}] (c) on the horizontal plane located at the elevation of the second blades from the bottom (z=63mm) at N=366 rpm.

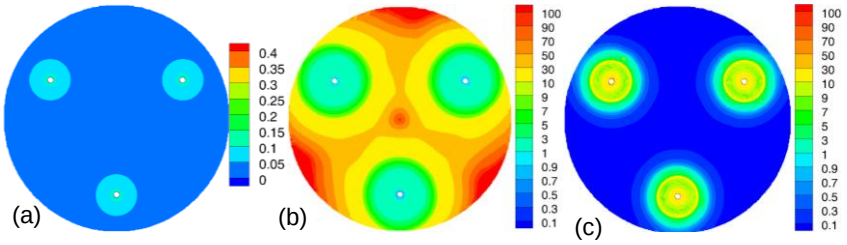

Figure 6: Predicted maps of the CMC solution velocity magnitude [m/s] (a), the viscosity [Pa·s] (b) and the shear rate [s^{-1}] (c) on the horizontal located at the elevation of the second blades from the bottom (z=63mm) at N=122rpm.

For gaining insight into the local values of the main variables affecting the biogas production in a condition which reproduces the production process, the results obtained considering the physical properties of the digestate and one of the two scale-down criteria are reported in Figure 7 and 8. The lower blades elevation is specifically selected in this case, being the fluid dynamics close to the vessel bottom often responsible of malfunctioning due to solid deposition.

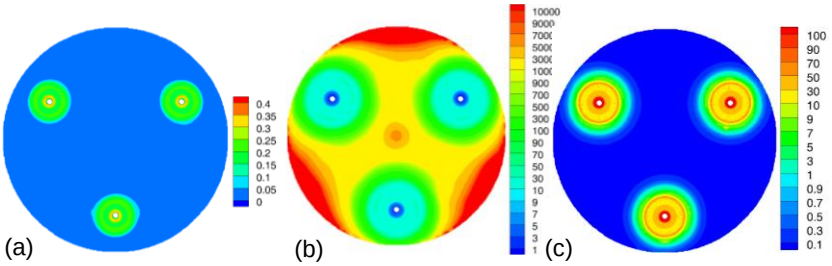

Figure 7: Predicted maps of the digestate velocity magnitude [m/s] (a), the viscosity [Pa·s] (b) and the shear rate [s^{-1}] (c) on the horizontal plane located at the lower blades elevation (z=30mm). N=366rpm.

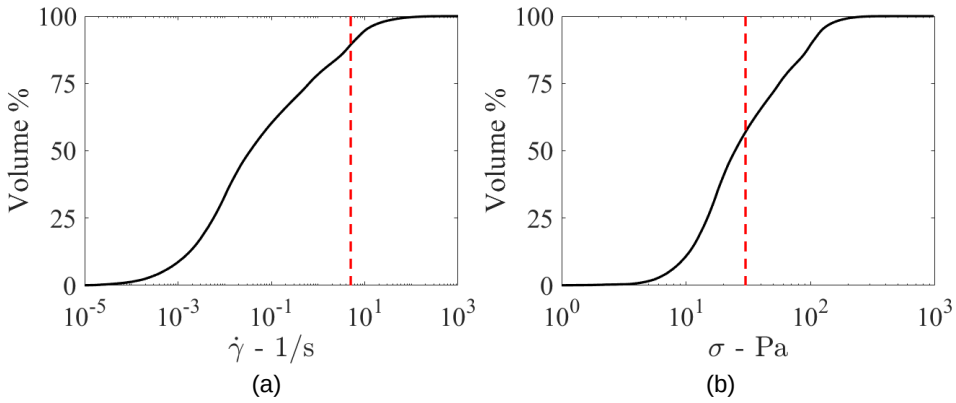

Figure 8: Cumulative distribution of shear rate (a) and shear stress (b) in the vessel volume. Fluid: digestate, N=366rpm.

The velocity magnitude map depicted in Figure 7(a) clearly shows that the fluid is almost stagnant in most of the vessel section, as a consequence of the fluid rheology, which leads to huge apparent viscosity values apart from the zone swept by the impeller, as shown in Figure 7(b). Considering previous results on the effect of agitation on biogas production (Lebranchu et al., 2017), significant improvement might be expected in the production process by a different choice of agitation system, at least in the case of the digestate considered in this work, for the following reasons:

- the calculated dead zones in the vessel exceed the 90%. Even higher values are expected using the constant shear rate criterion;

- the shear rate exceed the threshold of 5 s^{-1} that might provoke abrasion of the anaerobic sludge granules in a limited (Figure 7c), but not nil portion of the vessel, being about equal to 15% the volume of the vessel where this threshold is overcome (Figure 8a);
- the shear stress, which was found to be responsible of loss of productivity, is quite high in more than 50% of the vessel volume (Figure 8c).

3. Conclusions

The evaluation of the fluid dynamics features in a scale-down model digester considering the physical properties of the digestate and the geometry of a biogas production digester located in Emilia Romagna suggests that geometrical variation of the agitation system might lead to significant improvement of the production, based on the CFD prediction of dead zones, shear rate and shear stress and considering their impact on the biogas production rate estimated in previous investigations. Starting from the single-phase results presented in this work, the analysis will be extended to the identification of the most appropriate criterion to obtain similar dispersion dynamics and spatial distribution of the feedstock at different scales.

Nomenclature

D – impeller diameter, m
k_s – consistency index, Pa·s^{2-n}
N – impeller speed, 1/s
n – flow behaviour index, -
P – pressure, Pa
t – time, s
$\boldsymbol{u}$ – fluid velocity, m/s
u, v – cartesian velocity components, m/s
v_{tip} – impeller tip speed, m/s
$|V|$ – velocity magnitude, m/s
x, y, z – Cartesian coordinates
$\dot{\gamma}$ – shear rate, 1/s
μ_a – fluid apparent viscosity, Pa·s
ρ – fluid density, kg/m^3
σ – shear stress, Pa

References

Alberini, F., Maluta, F., Paglianti, A., Montante, G., 2023, Power Consumption and Fluid Mixing in a Scale-Down Geometry of a Stirred Digester for Biogas Production, ACS Engineering Au, DOI: 10.1021/acsengineeringau.2c00047.

Battista, F., Fino, D., Ruggeri, B., 2014, Polyphenols concentration's effect on the biogas production by wastes derived from olive oil production, Chemical Engineering Transactions, 38, 373-378.

Bridgeman, J., 2012, Computational fluid dynamics modelling of sewage sludge mixing in an anaerobic digester. Advances in Engineering Software, 44, 54-62.

Dabiri, S., Kumar, P., Ebner, C., Rauch, W., 2021, On the effect of biogas bubbles in anaerobic digester mixing, Biochemical Engineering Journal, 173, art. no. 108088.

Lebranchu, A., Delaunay, S., Marchal, P., Blanchard, F., Pacaud, S., Fick, M., Olmos, E., 2017, Impact of shear stress and impeller design on the production of biogas in anaerobic digesters, Bioresource Technology, 245, 1139-1147.

Leite, S.A.F., Leite, B.S., Ferreira, D.J.O., Baêta, B.E.L., Dangelo, J.V.H., 2023, The effects of agitation in anaerobic biodigesters operating with substrates from swine manure and rice husk, Chemical Engineering Journal, 451, art. no. 138533.

Maluta, F., Paglianti, A., Montante, G., 2019. RANS-based predictions of dense solid–liquid suspensions in turbulent stirred tanks, Chemical Engineering Research and Design, 147, 470-482.

Montante, G., Bakker, A., Paglianti, A., Magelli, F., 2006. Effect of the shaft eccentricity on the hydrodynamics of unbaffled stirred tanks, Chemical Engineering Science, 61, 2807-2814.

Moretta, F., Goracci, A., Manenti, F., Bozzano, G., 2022, Anaerobic co-Digestion Feedstock Blending Optimization, Chemical Engineering Transactions, 96, 295-300.

Scamardella, D., De Crescenzo, C., Marzocchella, A., Molino, A., Chianese, S., Savastano, V., Tralice, R., Karatza, D., Musmarra, D., 2019, Simulation and optimization of pressurized anaerobic digestion and biogas upgrading using aspen plus, Chemical Engineering Transactions, 74, 55-60.

Singh, B., Szamosi, Z., Siménfalvi, Z., 2019, State of the art on mixing in an anaerobic digester: A review, Renewable Energy, 141, 922-936.

Theuerl, S., Herrmann, C., Heiermann, M., Grundmann, P., Landwehr, N., Kreidenweis, U., Prochnow, A., 2019, The future agricultural biogas plant in Germany: A vision, Energies, 12 (3), art. no. 396.

Wichterle, K., Kadlec, M., Žák, L., Mitschka, P., 1984, Shear rates on turbine impeller blades, Chemical Engineering Communications, 26, pp. 25-32.